Monthly Notices
of the
ROYAL ASTRONOMICAL SOCIETY

MNRAS **463,** 2265–2272 (2016)
Advance Access publication 2016 August 26

doi:10.1093/mnras/stw2155

The peculiar dipping events in the disc-bearing young-stellar object EPIC 204278916

S. Scaringi,[1]★ C. F. Manara,[2] S. A. Barenfeld,[3] P. J. Groot,[4] A. Isella,[5] M. A. Kenworthy,[6] C. Knigge,[7] T. J. Maccarone,[8] L. Ricci[9] and M. Ansdell[10]

[1]*Max-Planck-Institute für Extraterrestriche Physik, D-85748 Garching, Germany*
[2]*Scientific Support Office, Directorate of Science, European Space Research and Technology Centre (ESA/ESTEC), Keplerlaan 1, NL-2201 AZ Noordwijk, the Netherlands*
[3]*Department of Astronomy, California Institute of Technology MC 249-17, Pasadena, CA 91125, USA*
[4]*Department of Astrophysics/IMAPP, Radboud University Nijmegen, PO Box 9010, NL-6500 GL Nijmegen, the Netherlands*
[5]*Department of Physics and Astronomy, Rice University, 6100 Main St Houston, TX 77005, USA*
[6]*Leiden Observatory, Leiden University, PO Box 9513, NL-2300 RA Leiden, the Netherlands*
[7]*School of Physics and Astronomy, University of Southampton, Hampshire SO17 1BJ, UK*
[8]*Department of Physics and Astronomy, Texas Tech University, Box 41051, Lubbock, TX 79409-1051, USA*
[9]*Harvard-Smithsonian Center for Astrophysics, 60 Garden Street, Cambridge, MA 02138, USA*
[10]*Institute for Astronomy, University of Hawai'i at Mānoa, Honolulu, HI 96822, USA*

Accepted 2016 August 23. Received 2016 August 19; in original form 2016 July 15

ABSTRACT

EPIC 204278916 has been serendipitously discovered from its *K2* light curve that displays irregular dimmings of up to 65 per cent for ≈25 consecutive days out of 78.8 d of observations. For the remaining duration of the observations, the variability is highly periodic and attributed to stellar rotation. The star is a young, low-mass (M-type) pre-main-sequence star with clear evidence of a resolved tilted disc from Atacama Large Millimeter/submillimeter Array (ALMA) observations. We examine the *K2* light curve in detail and hypothesize that the irregular dimmings are caused by either a warped inner disc edge or transiting cometary-like objects in either circular or eccentric orbits. The explanations discussed here are particularly relevant for other recently discovered young objects with similar absorption dips.

Key words: comets: general – planets and satellites: dynamical evolution and stability – stars: early-type – stars: individual: (EPIC 204278916) – stars: peculiar.

1 INTRODUCTION

Studies of light curves of stars are a proxy for several physical processes, both at the stellar surface or in their surroundings. Periodic variability of the observed stellar flux has long been used to measure stellar rotation periods (e.g. Stassun et al. 1999). Variability in young stellar objects (YSOs) is also related to the presence of a protoplanetary disc. Material in the disc can obscure the central star (e.g. Herbst et al. 1994; Alencar et al. 2010), and the highly variable accretion on to the central star modifies the emission from the system (e.g. Bertout, Basri & Bouvier 1988; Bouvier et al. 2007). The variability of YSOs is known to have different degrees of periodicity and flux symmetry that are possibly related to different processes (Cody et al. 2014). Recently, *CoRoT* and *Kepler*/*K2* observations of main-sequence stars and YSOs have shown deep and short dips in light curves that can be explained by the presence of a family of comets orbiting around the stars (Bodman & Quillen 2015; Boyajian et al. 2016) or more generally transiting circumstellar material (Ansdell et al. 2016b), or through occulting material at the inner edges of a circumstellar disc (McGinnis et al. 2015; Ansdell et al. 2016b). The latter is possible if the inner disc is observed almost edge on, and offers a unique opportunity to study the properties of dust and gas in the inner region of protoplanetary discs. If the dimming events are caused by transiting circumstellar clumps originating in the disc, these can be used to constrain the size of planetesimals in the disc, which is a necessary step for planet formation but difficult to observationally detect Testi et al. (2014).

More recently, Ansdell et al. (2016a) have found three YSO dippers with a wide range of inclination angles, demonstrating how edge-on discs are not a defining characteristic of dipping YSOs. At this stage, it is important to study a variety of dipper YSOs in detail and explore possible scenarios to explain their behaviour and their relevance for planet formation studies.

We have serendipitously discovered a YSO dipper star observed with *K2*, giving us the possibility to further investigate these peculiar systems. The target discussed here (EPIC 204278916, 2MASS J16020757−2257467) is a young star located in the Upper-Scorpius sub-group of the Scorpius–Centaurus (Sco–Cen) OB association (Preibisch & Mamajek 2008) with very high membership

★ E-mail: simo@mpe.mpg.de

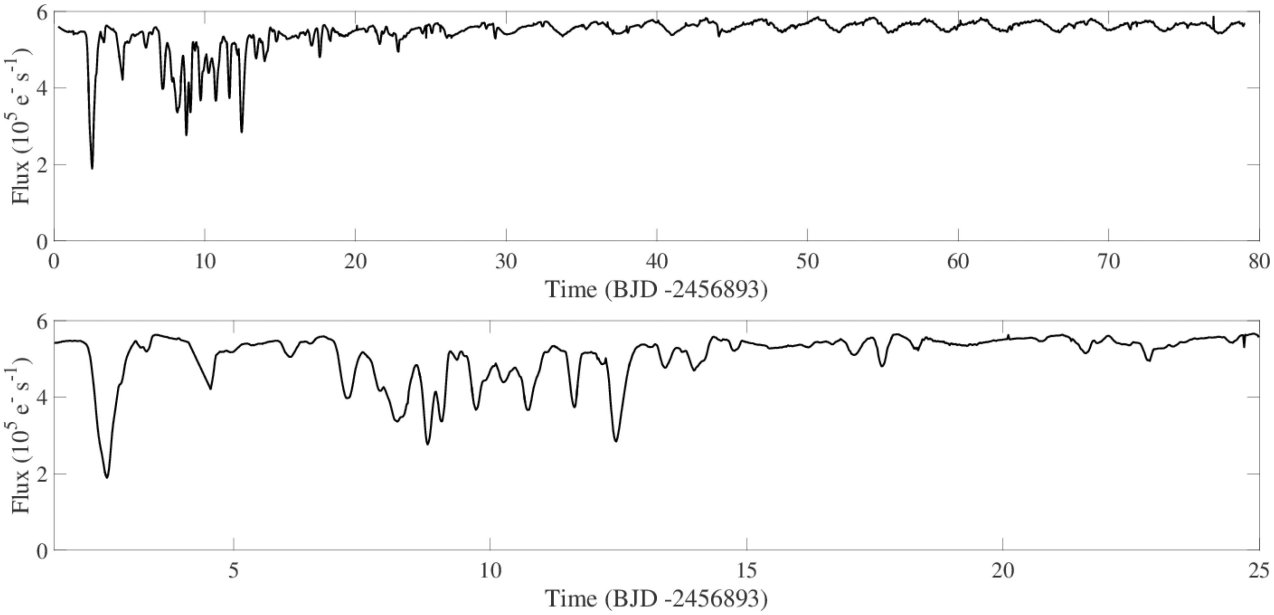

Figure 1. EPIC 204278916 light curve. The system was observed for over 78.8 d at 29.4 min cadence. The units on the *y*-axis are electrons per second, and can be converted to *Kepler* magnitudes *Kp* using the conversion found in the *Kepler* Instrument Handbook. The top panel shows the full light curve, whilst the bottom panel zooms into the first 25 d of observation where the dipping events are observed.

probability based on proper motion studies (99 per cent, Bouy & Martín 2009). This region has a mean age of ∼5 Myr (Preibisch et al. 2002, with an upper limit of ∼11 Myr; Pecaut, Mamajek & Bubar 2012). Our target is a single star (Kraus & Hillenbrand 2007) of spectral type M1 and has a logarithmic bolometric stellar luminosity $\log L_\star/\mathrm{L}_\odot = 0.15$ (Preibisch et al. 2002). The inferred radius of this star is $R_\star = 0.97\ \mathrm{R}_\odot$, while the stellar mass is $M_\star \sim 0.5\ \mathrm{M}_\odot$, depending on the evolutionary models used (Baraffe et al. 1998; Siess, Dufour & Forestini 2000).

At this age, the majority of young stars have already dispersed their circumstellar disc and are not accreting material from the disc anymore (e.g. Fedele et al. 2010). Spectroscopic observations of the H α line of this target report a very small equivalent width (EW $= -3.2$ Å, Preibisch et al. 2002), consistent with very little or no accretion. However, this target shows an infrared excess due to the presence of a protoplanetary disc in *Wide-field Infrared Survey Explorer* data (Luhman & Mamajek 2012).

The next section will introduce the *K2* and Atacama Large Millimeter/submillimeter Array (ALMA) data and the analysis procedure to obtain the reduced light curve (with corresponding Fourier transform) and the ALMA intensity map. Section 3 discusses the observations in the context of various interpretations, including a protostellar disc origin and cometary-like transits in either circular or eccentric orbits. We discuss our results in Section 4 and give our conclusions in Section 5 with future prospects for determining the real nature of EPIC 204278916.

2 DATA REDUCTION AND ANALYSIS

2.1 *K2* light curve

EPIC 204278916 was observed by the *K2* mission (Borucki et al. 2010) during Campaign 2 between 2014 August 23 and 2014 November 13 (78.8 d) and has a registered *Kepler* magnitude (*Kp*) of 13.8 in the *K2* Ecliptic Plane Input Catalog (EPIC). Here, we analyse long cadence (LC, 29.4 min) data obtained from the Mikulski Archive for Space Telescope (MAST) archive.[1] The data are provided in raw format, consisting of target pixel data. For each 29.4 min exposure, we thus have a 12 × 11 pixel image centred on the target.

As no other sources were present within the 12 × 11 pixel images, we create the light curve by manually defining a large target mask as well as a background mask. A large target mask is required due to occasional small-scale jittering of the spacecraft, resulting in the target moving slightly from its nominal position. The data set consists of 3856 individual target images. From these we remove 93 observations because of bad quality due to occasional spacecraft rolls or due to cosmic rays. We produce the light curve by summing together all target pixels for each exposure, and subtract the average background obtained from the background pixel mask. The obtained light curve is shown in Fig. 1. The same procedure has been used to extract other *K2* light curves of isolated sources (Scaringi et al. 2015a,b).

To locate any significant periodicities, we carry out a Fourier transform of the light curve excluding the first 30 days (in order to not be affected by the initial dipping period, see Fig. 1). Fig. 2 shows our result, revealing two distinct periodicities of 3.646 d ($F_1 = 0.2743$ cycles per day) and 0.245 d ($f_1 = 4.080$ cycles per day), together with corresponding harmonic frequencies. We associate the 3.646-d signal to stellar rotation, as this is a typical rotational period for young stars observed by *Kepler* (Vasconcelos & Bouvier 2015; Ansdell et al. 2016b), and show the phase-folded profile in Fig. 3. The 0.245-d signal is associated with the spacecraft thruster firing to re-adjust attitude every ∼6 h.

To study the dipping behaviour in more detail, we have removed the 3.646-d periodicity from the full light curve. To do this we first determined an accurate ephemeris of

$$\mathrm{BJD}_{\mathrm{min}} = 2456955.7082(18) + 3.646221(53) \times N, \quad (1)$$

[1] http://archive.stsci.edu/k2/

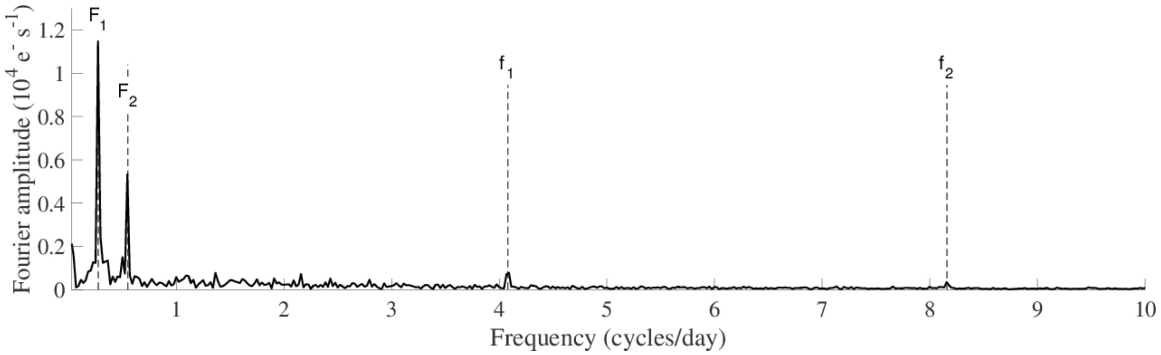

Figure 2. Fourier transform of LC *K2* data for EPIC 204278916 starting from day 25. A peak at $F_1 = 0.2743$ cycles per day (with corresponding harmonic F_2) is visible and at $f_1 = 4.080$ cycles per day (with corresponding harmonics f_2, f_3, f_4 and f_5). We associate F_1 to the possible stellar rotation, whilst f_1 can be attributed to spacecraft attitude adjustments.

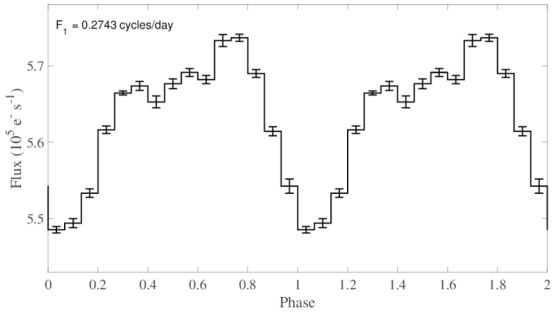

Figure 3. EPIC 204278916 light curve folded on the stellar rotation period of 3.646 d.

where N is the cycle number and the ephemeris is given in Barycentric Julian Date (BJD) at minimum light.

We then expand and replicate the phase-folded light curve shown in Fig. 3 to match the full light curve and interpolate it on the same temporal grid. Fig. 4 shows the full light curve with the 3.646-d periodicity removed. The periodicity removal is not perfect (probably due to small changes in the pulse profile over time) but shows a significant improvement over the original light curve. We use this curve in subsequent analysis.

2.2 ALMA observations

ALMA Cycle 2 observations of EPIC 204278916 were obtained on 2014 June 30 and 2014 July 7 (UT) in four spectral windows centred at 334.2, 336.1, 346.2 and 348.1 GHz for a mean frequency of 341.1 GHz (0.88 mm). The bandwidth of each window is 1.875 GHz. A total of 36 antennas were included in the array, with baselines ranging from 16 to 650 m for an angular resolution of 0.34 arcsec. The ALMA data were calibrated using the CASA package. The reduction scripts were kindly provided by National Radio Astronomy Observatory (NRAO). These include atmospheric calibration using the 183 GHz water vapour radiometers, bandpass calibration, flux calibration and gain calibration. For further details on the observations and data reduction, see Barenfeld et al. (2016). The protoplanetary disc in EPIC 204278916 is resolved with ALMA at high signal to noise, both in the continuum (see Fig. 5) and in the CO(J = 3−2) line (Barenfeld et al. 2016). An elliptical Gaussian fit of the surface brightness profile to the continuum visibility data results in an axis ratio of 0.55 ± 0.13, implying a disc inclination of 57 ± 9 degrees and assuming a circular disc.

3 RESULTS

In this section, we will go through possible scenarios to explain the observed large-amplitude dipping events in EPIC 204278916.

3.1 Protostellar disc origin

Provided with a favourable disc inclination, the observed dips in the EPIC 204278916 light curve could be caused by non-axisymmetric structures in the inner disc edge occulting the star. Because of the large observed dips (≈65 per cent), the occulting material must have a large scaleheight comparable to the size of the star. If the disc warps producing the occultations are orbiting the star with a Keplerian period equal to the stellar rotation, we can infer a maximum co-inclination (Ansdell et al. 2016b) in degrees

$$i_{\max} \lesssim 27 \frac{R_*}{\mathrm{R}_\odot} \frac{P_{\mathrm{rot}}}{\mathrm{d}}^{-2/3} \frac{M_*}{\mathrm{M}_\odot}^{-1/3}. \quad (2)$$

Adopting $P_{\mathrm{rot}} = 3.646$ d, $R_* = 0.97\,\mathrm{R}_\odot$ and $M_* = 0.5\mathrm{M}_\odot$, we obtain a maximum inclination $i_{\max} = 14$ degrees. This is somewhat in contrast with the 3σ level for the disc inclination of $i = 57$ degrees obtained from the ALMA image.

Other YSOs have been observed to display non-periodic dipping events (see e.g. Ansdell et al. 2016a,b; Sousa et al. 2016), and it is possible that EPIC 204278916 is also a part of this 'dipper' class of YSOs. In particular, EPIC 204278916 supports the idea that nearly edge-on viewing geometries are not a defining characteristic of dippers. This in turn motivates the exploration of alternative models. More specifically, the clustering of large-amplitude dipping events such as those observed in the *K2* EPIC 204278916 light curve have not been previously observed in other systems. The only other YSO dipper that appears to resemble EPIC 204278916 as observed with *K2* is EPIC 204530045 (see fig. 1 of Bodman et al. 2016). However, on close inspection, it appears that the dipping behaviour between EPIC 204278916 and EPIC 204530045 differs in that (i) the dips in EPIC 204278916 always appear to return to the stellar flux whilst there is a clear downward general trend for EPIC 204530045, (ii) whilst EPIC 204278916 solely displays dipping, the light curve of EPIC 204530045 more resembles flickering and (iii) the dip depth is nearly a factor of 3 larger for EPIC 204278916 when compared to EPIC 204530045. All three arguments seem to suggest that whilst the *K2* light curves of both EPIC 204278916 and EPIC 204530045 appear similar, the phenomenology observed in EPIC 204530045 seems to be accretion driven (change in instantaneous mass transfer rate on the stellar surface), whilst EPIC 204278916 has all the

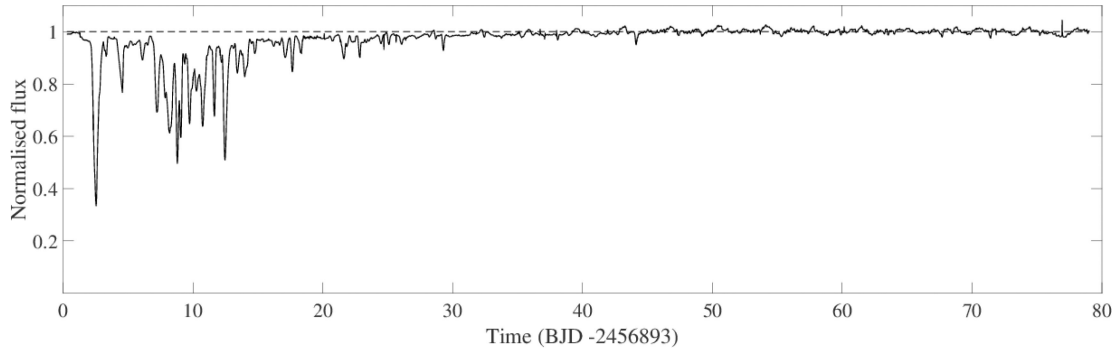

Figure 4. Normalized EPIC 204278916 light curve with the 3.646-d periodicity removed.

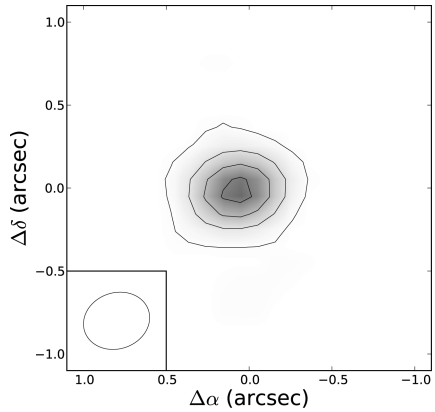

Figure 5. ALMA continuum intensity map for EPIC 204278916. Isocontours for 3σ, 10σ, 17σ and 23σ are overlaid on the image. The ALMA beam size is shown in the bottom-left corner.

characteristics of being 'transited'. Thus, if EPIC 204278916 is also a part of the YSO 'dipper' class as those discussed in Bodman et al. (2016), then it constitutes a somewhat special case.

3.2 Hill sphere ring system

The rapid fluctuations over the first 25 d of observations are similar to those seen towards J1407, another young star in the Sco–Cen association. In 2007 May, a series of rapid fluctuations was seen over a 56-d period (Mamajek et al. 2012) and interpreted as a giant ring system filling the Hill sphere of the unseen secondary companion (Kenworthy & Mamajek 2015; Kenworthy et al. 2015). The series of dips after the first initial deep dip show hints of being symmetric in time, around $T = 10$ d in Fig. 6 (bottom panel), consistent with a ring system that is inclined with respect to our line of sight. The gradient of the light curve of such an inclined ring system will show small gradients near the point of closest projected approach as the star moves parallel to ring edges, and steeper light-curve gradients at other times. This is not seen in the gradient of the light curve as a function of time (Fig. 6, top panel), and so this is considered an unlikely hypothesis for these dips.

3.3 Transiting circumstellar clumps

It is possible that the dips in some YSOs might be caused by transiting circumstellar objects, similar to what has been proposed for KIC 8462852 (Bodman & Quillen 2015; Marengo, Hulsebus & Willis 2015; Boyajian et al. 2016). The discussion presented below is tailored to the dipping YSO EPIC 204278916, but can be extended to other dipping YSOs such as those discussed in Ansdell et al. (2016a).

3.3.1 Transiting material in circular orbit

With the assumption that the transiting object(s) are in circular orbits, we can place tight constraints on the orbital parameters in a plane defined by the semimajor axis (a) and the transiting clump radius (R_c). These are included in Fig. 7, and described in detail below.

Dip depth: constraints on the clump size can be obtained from the dip depth τ, defined as 1 minus the normalized absorbed flux during the dipping event (see Fig. 4). In the most extreme scenario, where the eclipsing clump is completely opaque, $\max(\tau) = (R_c/R_*)^2$. The deepest event observed in the EPIC 204278916 light curve corresponds to $\tau \approx 65$ per cent, thus implying that at least some of the clumps are a sizable fraction of the parent star. This is however a strong lower limit since a completely opaque spherical clump would produce a symmetrical dip, which we do not observe in the light curve (see Fig. 1).

Dip duration: a transiting object will have a transverse velocity along the stellar equator of

$$v_t = \frac{2(R_c + R_*)}{t_{dip}}, \tag{3}$$

where t_{dip} is the transit duration. If the object is on a circular orbit around a star of mass M_* with semimajor axis a, then we can estimate the size of the transiting object with

$$R_c = \frac{t_{dip}}{2}\left(\frac{GM_*}{a}\right)^{1/2} - R_*. \tag{4}$$

Thus, the observed dip durations in the EPIC 204278916 light curve can provide an estimate for the transiting clump size for circular orbits. The longest dip duration of $t_{dip} = 1$ d provides the most stringent constraint, and is shown as a solid black line in Fig. 7.

Light-curve gradient: an outer constraint on the semimajor axis can be derived using the largest gradient observed during a transit event. Transiting material will change the light curve most rapidly when it is optically thick and transiting through the stellar equator. van Werkhoven, Kenworthy & Mamajek (2014) provide the equation required to translate the observed gradients into a minimum velocity (v_{min}) for transiting material using the so-called knife edge model. Assuming then that the material is in a circular orbit and optically thick, the obtained minimum velocity constraint of 39 km s^{-1} translates to a maximum semimajor axis of 0.2916 au through

$$a_{max} = \frac{GM_*}{v_{min}^2}. \tag{5}$$

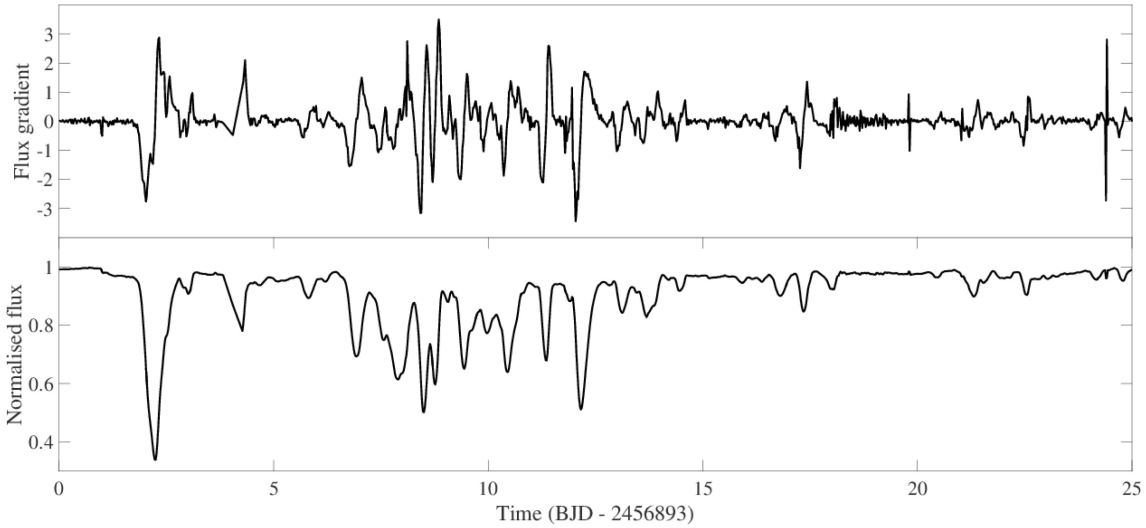

Figure 6. Bottom panel: normalized EPIC 204278916 light curve (with the 3.646-d periodicity removed) for the first 25 d of observation. Top panel: corresponding light-curve gradient.

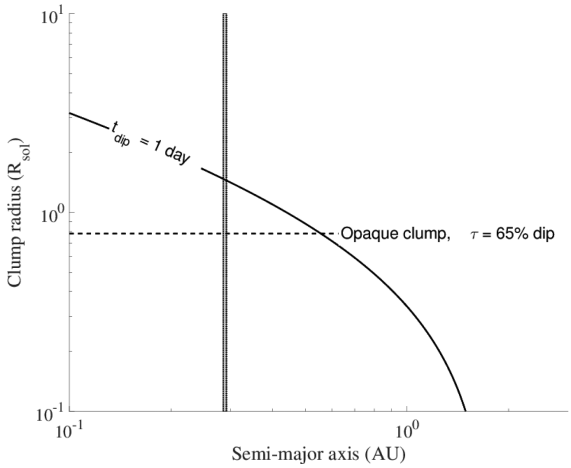

Figure 7. Assuming 1-d dips, the figure shows the possible semimajor axis versus clump radius values with the solid black line. The minimum clump size, obtained through the observed dip amplitude, is shown with the dashed line. The two vertical dotted lines show the minimum and maximum semimajor axis obtained with the non-periodicity and observed minimum velocity (for optically thick material) constraint, respectively.

Non-periodicity: given that we do not observe a repetition of the dipping events within the total light curve, we can place a constraint on the orbital period to be longer than 78.8 d. This in turn sets a lower limit on the semimajor axis of 0.2855 au for circular orbits.

All constraints for circular orbits are displayed in Fig. 7. The very tight semimajor axis constraints raise some doubts on this interpretation, since they imply that the orbital period of the transiting material is just slightly longer than the 78.7 d *K2* observations. Furthermore, it is possible that the dipping events began before the start of the *K2* observations, in which case circular orbits would be fully ruled out. It is also important to note that the resulting size for the transiting clump would be very large at $R_c \approx 1.5 R_{sol}$.

3.3.2 Transiting material in eccentric orbit

ALMA observations have revealed the inclination of the circumstellar disc to be 57 ± 9 degrees. It is thus plausible that the transiting material orbits out of the disc plane, in which case its motion does not need to be constrained to a circular orbit. Introducing an eccentric orbit is far less constraining than assuming circular orbits. We can nevertheless use the observed minimum velocity (obtained through the light-curve gradient) and the minimum semimajor axis (obtained through the non-periodicity of the dips) to provide some constraints.

For eccentric orbits with eccentricity e, the orbital velocity at pericentre and apocentre, respectively, are defined as

$$v_{\rm per} = \sqrt{GM_* \frac{1+e}{a(1-e)}} \tag{6}$$

and

$$v_{\rm apo} = \sqrt{GM_* \frac{1-e}{a(1+e)}}. \tag{7}$$

Fig. 8 shows these velocities as a function of eccentricity adopting the derived minimum semimajor axis of $a_{\rm min} = 0.2855$ au. The obtained velocities represent maximum velocities at both pericentre and apocentre, since increasing the semimajor axis will result in lower velocities. Plotted in Fig. 8 is the observed minimum velocity of $v_{\rm min} = 39\,{\rm km\,s^{-1}}$ obtained from the light-curve gradient of the dips. This already shows that if the orbit is eccentric, then we are most likely observing the transit away from apocentre.

We can further expand on this analysis and speculate what the eccentricity would be if the transiting material has broken into smaller clumps due to a close passage to its parent star at pericentre. The pericentre and apocentre radii, respectively, are given by

$$r_{\rm per} = a(1-e) \tag{8}$$

and

$$r_{\rm apo} = a(1+e). \tag{9}$$

Fig. 9 shows these radii as a function of eccentricity adopting the same minimum semimajor axis as used in Fig. 8. The obtained radii in this case can be thought of as lower limits, since increasing the semimajor axis will result in larger pericentre and apocentre radii. The dashed line in Fig. 9 shows the Roche radius below which a cometary-like object with a density of 0.5 g cm^{-3} would break up.

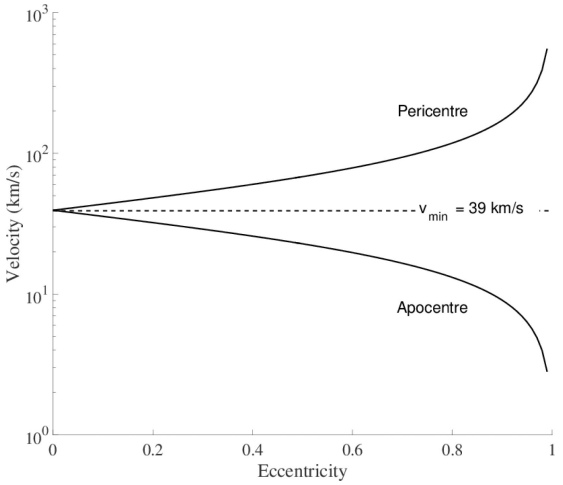

Figure 8. Pericentre and apocentre orbital velocities for varying eccentricities with a constant semimajor axis of $a = 0.2855$ (solid black lines). The dashed horizontal line marks the observed minim velocity of 39 km s^{-1}. If the observed dips in EPIC 204278916 are caused by transiting material on an eccentric orbit, then the observed transit must occur away from apocentre.

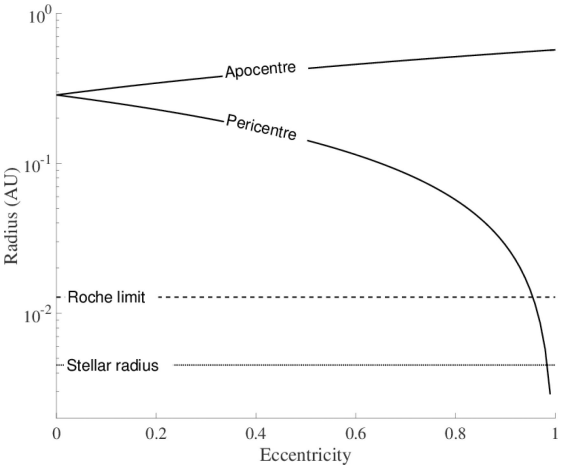

Figure 9. Pericentre and apocentre radii for varying eccentricities adopting the observed minimum semimajor axis of $a = 0.2855$ au. The dashed line marks the Roche radius below which a large cometary-like body with density $\rho = 0.5$ gm cm^{-3} would break up. The dotted line marks the stellar radius, below which orbiting clumps would crash into the star. For this scenario, the eccentricity can be constrained to be above 0.95.

The eccentricity would have to be very large ($e > 0.95$) for this case, and might resemble the Comet Shoemaker–Levy 9 event that broke apart and collided with Jupiter in 1994 July (see e.g. Chodas & Yeomans 1996).

3.3.3 *Mass constraint of transiting clumps*

We can place a lower constraint on the mass of the transiting material (independent of eccentricity) by assuming that the observed individual dips are caused by a cluster of objects, each of a different mass and size. The mass of each clump is defined by

$$M = m_{\rm g} \rho V, \tag{10}$$

where $m_{\rm g}$ is the average grain mass, ρ the object density and V its volume. In turn the volume can be estimated by

$$V = \pi R_{\rm c}^2 \Delta R, \tag{11}$$

where ΔR is the clump depth along the line of sight. We can obtain an estimate on $R_{\rm c}$ from the observed dip depths, but it is non-trivial to obtain ΔR. However, from the definition of optical depth (τ) we find that

$$\tau = \rho \sigma \Delta R, \tag{12}$$

where σ is the cross-section of the particles causing the obscuration. Through some algebraic manipulation, we can substitute equations (12) and (11) into equation (10) to obtain

$$M = \frac{m_{\rm g} \pi R_{\rm c}^2 \tau}{\sigma}, \tag{13}$$

and note that both the density and clump depth cancel out. Equation (13) is useful in obtaining a lower mass limit on the transiting material, since we know the minimum clump radii from the dip depths and also that $\tau \geq 1$. The only unconstrained parameters are the cross-section σ and the grain mass $m_{\rm g}$, which we fix to 10^{-8} cm^2 and 10^{-14} grams, respectively, typical for dust grain sizes of $\approx$0.1 μm. These values should be regarded as lower limits from derived dust grain mass distributions (e.g. Li & Greenberg 1998).

To obtain the number and radius of the transiting clumps, we perform a multiGaussian fit to the EPIC 204278916 light curve (after removing the 3.646-d periodicity) as shown in Fig. 4. Using a local peak finding algorithm (FINDPEAK implemented in MATLAB), we identify 53 dips. Fig. 10 shows the first 25 d of observations fitted with 53 Gaussians of differing widths and amplitudes and one broad Poisson function covering the timespan of the smaller dips. We find that the Poisson component is necessary to obtain a good fit to the data, but that the goodness-of-fit is not sensitive to the exact number of Gaussians used. For each Gaussian component, we obtain the related $R_{\rm c}$ and estimate the mass of each individual component using equation (13). The sum of all Gaussians then yields a reasonable lower mass limit for the whole clump of $M_{\rm c} = 7 \times 10^{17}$ grams ($\approx$3.2 times the mass of Halley's Comet).

4 DISCUSSION

The large-amplitude dipping events observed in the *K2* light curve of EPIC 204278916 superficially resemble other systems recently discovered with *K2*. Most notably, KIC 8462852 (Boyajian et al. 2016) was observed to have similar dip durations to those observed in EPIC 204278916. However, aside from this, KIC 8462852 and EPIC 204278916 differ in many other respects. First, EPIC 204278916 shows much deeper dips than KIC 8462852. Furthermore, the dipping patterns observed in EPIC 204278916 are clustered in time, with an initial deep dipping event being followed by smaller ones for $\approx$25 d before returning to the normal, presumably quiescent state of the star. The dips observed in KIC 8462852 are not clustered, but are spread out over a period of several years. More importantly however, KIC 8462852 displays an ordinary F-type star spectrum (Boyajian et al. 2016) showing no accretion signatures, whilst EPIC 204278916 is a YSO still surrounded by a disc, based on both the ALMA images shown in this work (Fig. 5), its spectral features (e.g. presence of lithium absorption line and Hα emission line, Preibisch et al. 2002), and its membership in the Sco–Cen OB association (Preibisch & Mamajek 2008).

More recently, Ansdell et al. (2016a) have discovered three objects which more resemble EPIC 204278916 when compared to KIC 8462852. These also belong to the Upper-Scorpius association and are YSOs. Similar to what has been presented here for EPIC 204278916, Ansdell et al. (2016a) have resolved the discs with ALMA, and demonstrated that large-amplitude dipping events are

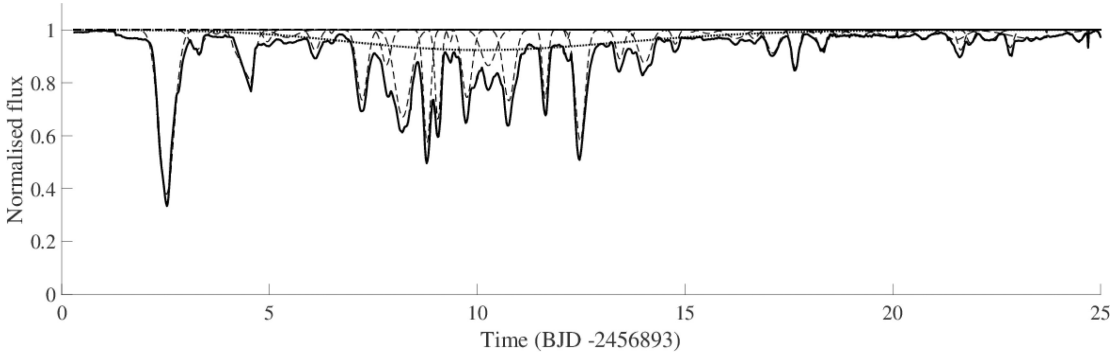

Figure 10. Normalized EPIC 204278916 light curve (solid line, with the 3.646-d periodicity removed) decomposed into 53 Gaussians (dashed lines) and one Poissonian component (dotted line).

not only observed in edge-on systems. Given that both the objects presented by Ansdell et al. (2016a) and EPIC 204278916 belong to the same star-forming association, and all show large dipping events, one might consider them to be part of the same class of dipping systems. However, the peculiarly clustered dipping structure displayed by EPIC 204278916 distinguishes it from previously reported YSO dipping systems. The only exception might be EPIC 204530046 (presented in Bodman et al. 2016), although we discussed in Section 3.1, why we think EPIC 204278916 is qualitatively different.

Given the large range of inclination angles inferred from the resolved ALMA images of EPIC 204278916 and the sample of Ansdell et al. (2016a), it is unlikely that the observed dips are related to the outer edges of the protostellar disc. It is however possible that an inclined and variable inner dust disc could cause some of the observed dips (see e.g. HD 142527, Marino, Perez & Casassus 2015). This is particularly relevant for some of the systems discussed in Ansdell et al. (2016a) and Bodman et al. (2016), where the dipping events are observed to persist throughout the full ≈3 months of *K2* observations and some display quasi-periodic dips that repeat on the period of the stellar co-rotation radius. If a similar mechanism were responsible for the observed dips in EPIC 204278916, the inclined inner disc would have to be transient on a relatively short time-scale of a few weeks, making this interpretation also unlikely. Furthermore, we find no relation between the repeating dip patterns in EPIC 204278916 with the stellar rotation. Thus, both the transient nature of the observed dips and the fact that they do not repeat (quasi-)periodically makes EPIC 204278916 stand out even more from previously observed YSO dippers.

In Section 3.3, we explored the possibility that the observed dips in EPIC 204278916 are caused by transiting circumstellar clumps. We showed how circular orbits for this interpretation are most likely ruled out and that highly eccentric orbits are consistent with the observations. If transiting cometary-like bodies are responsible for the observed dips, the events are most likely occurring close to periastron passage. If the dips are the result of a previous disruptive event of a larger body, we can further say that the eccentricity needs to be larger than 0.95 for previous pericentre passages to be within the Roche radius of the parent star. Similar disruptive events have been witnessed in our Solar system (e.g. Comet Shoemaker–Levy 9), but have never been previously witnessed around other stars. Thus, EPIC 204278916 could constitute the first system where a planetesimal-sized body has been witnessed to be tidally disrupted by the parent star upon a close encounter. This would be then a direct evidence of the presence of km-sized bodies in a protoplanetary disc, a crucial step towards planet formation.

Given there is no complete explanation for the mysterious behaviour of EPIC 204278916, more observations and modelling of this system are required to fully explain the clustered large-amplitude dipping events. Continuous photometric monitoring of this system for subsequent dipping events will determine whether this behaviour is periodic or not. Given the dynamics of break-up orbits, we would expect the cometary-like bodies to only survive a few orbits before hitting the parent star. It is thus important to monitor EPIC 204278916 before such an event occurs.

5 CONCLUSION

We have presented the *K2* light curve of the disc-bearing YSO EPIC 204278916, together with a resolved ALMA image constraining its disc inclination to 57 ± 9 degrees. The *K2* light curve displays prominent, large-amplitude dips during the first ≈25 d of observations out of the 78.8 d *K2* observing campaign. Although difficult to establish their true physical origin, we have discussed the observed dips in terms of a warped inner disc transiting circumstellar clumps in circular orbits, and cometary-like debris in an eccentric orbit.

It is clear that further observations of EPIC 204278916 and other YSO dippers will be required in the future, both photometric and spectroscopic, in order to establish their true origin. In particular, it is important to determine whether the observed dips in the *K2* light curve of EPIC 204278916 are observed again, in which case infer their recurrence time-scale and spectroscopic properties. In this respect, we point out the possibility of *K2* to re-observe part of the Sco–Cen OB association in 2017 during the planned Campaign 15.

ACKNOWLEDGEMENTS

We gratefully thank the anonymous referee for providing useful and insightful comments which have improved this manuscript. SS acknowledges funding from the Alexander von Humboldt Foundation. CFM acknowledges ESA research fellowship funding. This research has made use of NASA's Astrophysics Data System Bibliographic Services. Additionally, this work acknowledges the use of the astronomy and astrophysics package for MATLAB (Ofek 2014). This paper includes data collected by the *Kepler* mission. Funding for the *Kepler* mission is provided by the NASA Science Mission Directorate. Some of the data presented in this paper were obtained from the Mikulski Archive for Space Telescopes (MAST). STScI is operated by the Association of Universities for Research in Astronomy, Inc., under NASA contract NAS5-26555. Support for MAST for non-*HST* data is provided by the NASA Office of Space

Science via grant NNX13AC07G and by other grants and contracts. This paper additionally makes use of the following ALMA data: ADS/JAO.ALMA#2013.1.00395.S. ALMA is a partnership of European Southern Observatory (ESO, representing its member states), NSF (USA) and NINS (Japan), together with NRC (Canada) and NSC and ASIAA (Taiwan), in cooperation with the Republic of Chile. The Joint ALMA Observatory is operated by ESO, AUI/NRAO and NAOJ. This material is based upon work supported by the National Science Foundation Graduate Research Fellowship under Grant No. DGE-1144469.

REFERENCES

Alencar S. H. P. et al., 2010, A&A, 519, A88
Ansdell M., Gaidos E., Williams J. P., Kennedy G., Wyatt M. C., LaCourse D. M., Jacobs T. L., Mann A. W., 2016a, MNRAS, 462, L101
Ansdell M. et al., 2016b, ApJ, 816, 69
Baraffe I., Chabrier G., Allard F., Hauschildt P. H., 1998, A&A, 337, 403
Barenfeld S. A., Carpenter J. M., Ricci L., Isella A., 2016, ApJ, 827, 142
Bertout C., Basri G., Bouvier J., 1988, ApJ, 330, 350
Bodman E. H. L., Quillen A., 2015, ApJ, 819, L34
Bodman E. H. L. et al., 2016, MNRAS, preprint (arXiv:1605.03985)
Borucki W. J. et al., 2010, Science, 327, 977
Bouvier J. et al., 2007, A&A, 463, 1017
Bouy H., Martín E. L., 2009, A&A, 504, 981
Boyajian T. S. et al., 2016, MNRAS, 457, 3988
Chodas P. W., Yeomans D. K., 1996, in Noll K. S., Weaver H. A., Feldman P. D., eds, IAU Colloq. 156: The Collision of Comet Shoemaker-Levy 9 and Jupiter. Cambridge Univ. Press, Cambridge, p. 1
Cody A. M. et al., 2014, AJ, 147, 82
Fedele D., van den Ancker M. E., Henning T., Jayawardhana R., Oliveira J. M., 2010, A&A, 510, A72
Herbst W., Herbst D. K., Grossman E. J., Weinstein D., 1994, AJ, 108, 1906
Kenworthy M. A., Mamajek E. E., 2015, ApJ, 800, 126
Kenworthy M. A. et al., 2015, MNRAS, 446, 411
Kraus A. L., Hillenbrand L. A., 2007, ApJ, 662, 413
Li A., Greenberg J. M., 1998, ApJ, 498, L83
Luhman K. L., Mamajek E. E., 2012, ApJ, 758, 31
Mamajek E. E., Quillen A. C., Pecaut M. J., Moolekamp F., Scott E. L., Kenworthy M. A., Collier Cameron A., Parley N. R., 2012, AJ, 143, 72
Marengo M., Hulsebus A., Willis S., 2015, ApJ, 814, L15
Marino S., Perez S., Casassus S., 2015, ApJ, 798, L44
McGinnis P. T. et al., 2015, A&A, 577, A11
Ofek E. O., 2014, Astrophysics Source Code Library, record ascl:1407.005
Pecaut M. J., Mamajek E. E., Bubar E. J., 2012, ApJ, 746, 154
Preibisch T., Mamajek E., 2008, in Reipurth B., ed., The Nearest OB Association: Scorpius-Centaurus (Sco OB2), Handbook of Star Forming Regions, Volume II: The Southern Sky ASP Monograph Publications, Vol. 5, p. 235
Preibisch T., Brown A. G. A., Bridges T., Guenther E., Zinnecker H., 2002, AJ, 124, 404
Scaringi S. et al., 2015a, Sci. Adv., 1, e1500686
Scaringi S., Maccarone T. J., Hynes R. I., Körding E., Ponti G., Knigge C., Britt C. T., van Winckel H., 2015b, MNRAS, 451, 3857
Siess L., Dufour E., Forestini M., 2000, A&A, 358, 593
Sousa A. P. et al., 2016, A&A, 586, A47
Stassun K. G., Mathieu R. D., Mazeh T., Vrba F. J., 1999, AJ, 117, 2941
Testi L. et al., 2014, in Beuther H., Klessen R. S., Dullemond C. P., Henning T., eds, Protostars and Planets VI. Univ. Arizona Press, Tucson, p. 339
van Werkhoven T. I. M., Kenworthy M. A., Mamajek E. E., 2014, MNRAS, 441, 2845
Vasconcelos M. J., Bouvier J., 2015, A&A, 578, A89

This paper has been typeset from a TEX/LATEX file prepared by the author.